frontiers | Frontiers in Materials

TYPE Original Research
PUBLISHED 01 October 2025
DOI 10.3389/fmats.2025.1677367

OPEN ACCESS

EDITED BY
Antonios Kanellopoulos,
University of Hertfordshire, United Kingdom

REVIEWED BY
Amir Ali Shahmansouri,
Washington State University, United States
Jun-Jie Zeng,
Guangdong University of Technology, China

*CORRESPONDENCE
Xiang Liu,
liuxiang@fjut.edu.cn

RECEIVED 31 July 2025
ACCEPTED 01 September 2025
PUBLISHED 01 October 2025

CITATION
Yi S, Tang Z, Liu X and Chen H (2025) Flexural capacity of fiber reinforced polymer sea sand seawater concrete: reliability analysis and calibration of partial factor.
Front. Mater. 12:1677367.
doi: 10.3389/fmats.2025.1677367

Flexural capacity of fiber reinforced polymer sea sand seawater concrete: reliability analysis and calibration of partial factor

Shixiang Yi[1], Zhongping Tang[1], Xiang Liu[2]* and Hao Chen[2]

[1]Institute of Structural Material Failure and Strengthening Technology, Ningbo Polytechnic University, Ningbo, Zhejiang, China, [2]School of Civil Engineering, Fujian University of Technology, Fuzhou, China

Due to its efficient use of marine resources, seawater sea-sand concrete (SWSSC) has emerged as a promising sustainable building material and has garnered significant interest. At the same time, fiber reinforced polymer (FRP) materials show great potential for application in SWSSC structures owing to their excellent mechanical properties and corrosion resistance. However, the behavior of SWSSC is more uncertain compared to conventional concrete, which affects the reliability of structural members in terms of load-bearing capacity. To ensure the safety and reliability of FRP-SWSSC members, a database of 49 flexural tests on FRP-reinforced SWSSC beams was compiled to characterize the statistical distribution of the concrete material and the error associated with the computational model. Based on this data, a reliability analysis was conducted and a reliability model was developed. The partial factors were calibrated according to the target reliability index, resulting in recommended values of 1.4 for the Chinese code, 1.6 for ACI, 1.5 for CSA, and 1.3 for Eurocode.

KEYWORDS

sea water sea sand concrete beams, fiber-reinforced polymer (FRP), flexural capacity, reliability analysis, partial factor

1 Introduction

In recent years, the large-scale construction activities have led to a severe shortage of river sand resources, and the price of river sand has been continuously rising (Wang et al., 2023). At the same time, the global consumption of fresh water for preparing concrete amounts to about 2 billion tons annually (Miller et al., 2018), which has become an increasingly serious issue. Therefore, the using of sea water and sea-sand have attracted the attention of scholars.

The chemical and physical properties of sea sand vary significantly due to geographical factors. Chemically, research by Dhondy et al. (2024) indicated that the chloride ion content in sea sand is generally higher than that in river sand. The silicon content in sea sand can vary due to the presence of shells and organic materials, but it typically exceeds that of river sand. In terms of physical properties, Supplementary Appendix 1 compiles fineness modulus data for sea sand from various regions. The particle size distribution of sea sand varies by region. However, it generally complies with the second-class sand standards outlined in the

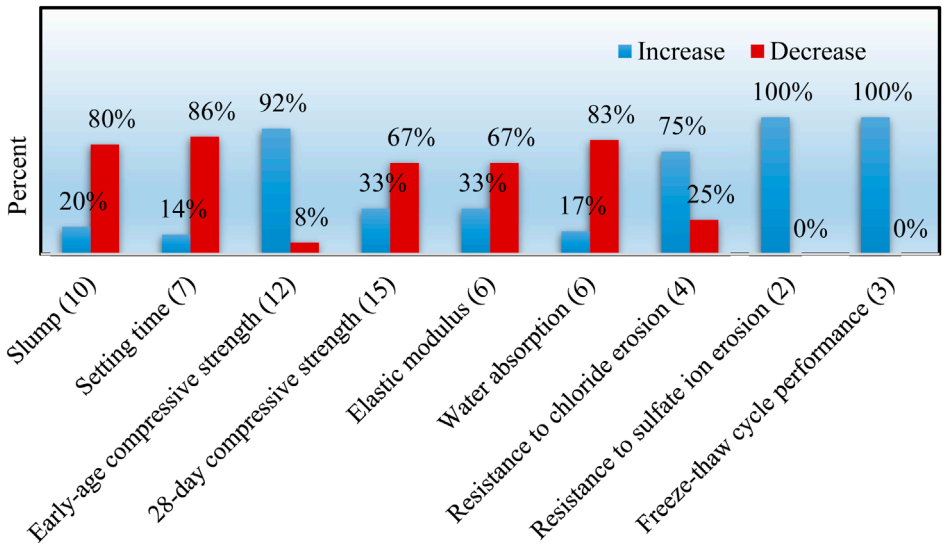

FIGURE 1
Difference between seawater sea sand concrete and river water river sand concrete.

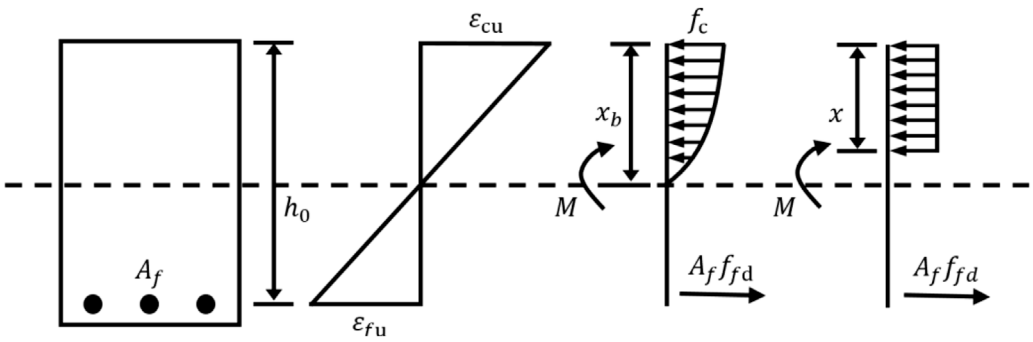

FIGURE 2
Stress-strain distribution of the tensile failure section.

guideline (GB/T14684-2011, 2011). The fineness modulus and particle size distribution of second-class sand meet the requirements for concrete mixing, making it an ideal material for concrete production.

The research on seawater sea-sand concrete (SWSSC) primarily focuses on its mechanical properties, durability, and issues related to rebar corrosion. Figure 1 synthesizes findings from 29 previous studies, illustrating the differences between SWSSC and ordinary concrete (OPC) in terms of slump, setting time, early compressive strength, 28-day compressive strength, elastic modulus, water absorption, resistance to chloride ion penetration, resistance to sulfate ion attack, and freeze-thaw durability. In this figure, the blue bars indicate improvements of SWSSC over OPC in certain metrics, while the red bars denote declines in other areas. The numbers in parentheses next to the axis labels represent the number of references cited.

In studies of mechanical properties, numerous findings indicate that concrete made with seawater sea sand experiences a slight increase in compressive strength during the first 7 days compared to freshwater river sand concrete (Pan et al., 2021). However, after 28 days of curing, its compressive strength typically falls below that of freshwater river sand concrete (Panchanathan and Paramasivam, 2022). The initial and final setting times of concrete, as well as its workability, significantly affect the construction methods and timeline of concrete structures. Most studies indicated (Lu et al., 2023a) that the initial and final setting times of SWSSC are shorter than those of freshwater river sand concrete.

Fiber-reinforced polymer (FRP) bars have been proposed as an ideal alternative. FRP bars, known for their lightweight, high strength, corrosion resistance, and fatigue resistance, are considered an ideal reinforcement material (Mai et al., 2023; Zeng et al., 2022). Their excellent corrosion resistance can effectively resist the erosion of chloride ions and moisture and oxygen in the air, thereby significantly improving the durability and reliability of concrete structures. Researchers had conducted various studies on FRP-reinforced concrete specimens, for examples,

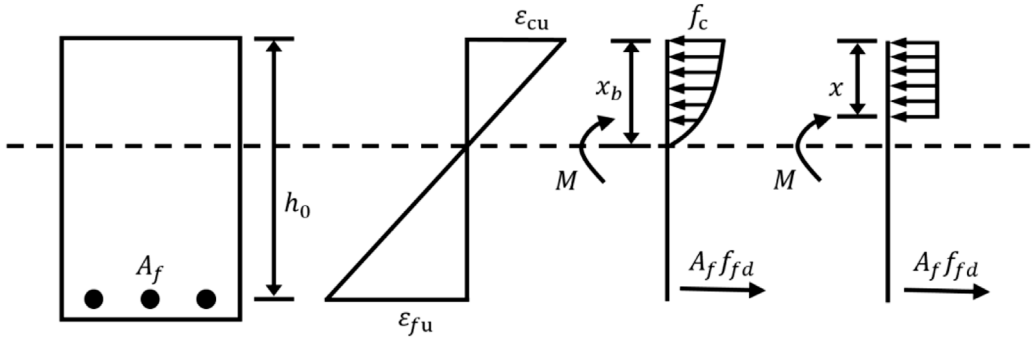

FIGURE 3
Stress-strain distribution of the boundary failure section.

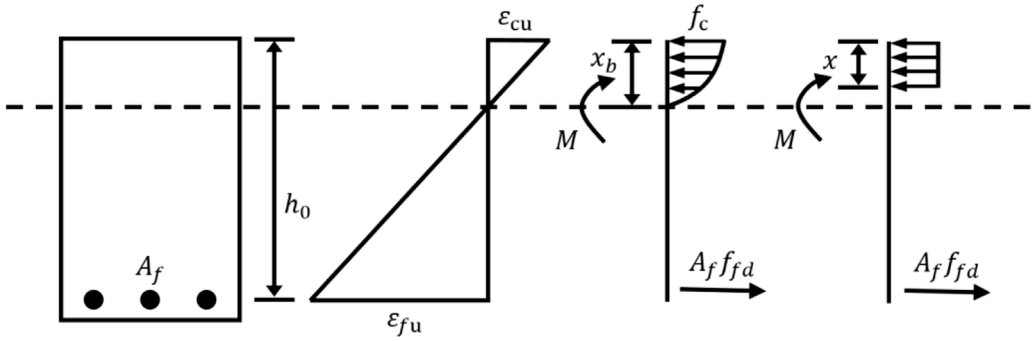

FIGURE 4
Stress-strain distribution of the compressive failure section.

TABLE 1 Environmental reduction factor for FRP, γe.

Environmental Conditions	FRP type	γe
Indoors	CFRP	1.00
	BFRP	1.00
	GFRP	1.25

Jafari et al. (2025) presented experimental and analytical insights into hybrid FRP systems and may provide useful comparative data or modeling strategies relevant to the current study's treatment of FRP types (CFRP, GFRP, BFRP). Zeng et al. (2025) FRP-3D printed concrete analyzed the bond performance between FRP bars and 3D-printed high-performance concrete. In addition, there are some related studies, such as the bond-slip behavior of FRP bars (Fahmy et al., 2021), steel-FRP (SFCB) composite bar concrete columns (Han et al., 2023), FRP bar and steel bar hybrid-reinforced concrete beams (Hussein et al., 2022), FRP fabric-reinforced concrete beams (Liao et al., 2022), FRP and steel bar-reinforced concrete slabs (Wang et al., 2020), FRP-confined concrete cylinders (Wu et al., 2006), long-term bond performance of FRP- concrete (Zhang et al., 2025), FRP- UHPC foundation (Fan et al., 2025a), and FRP-UHPC beam (Fan et al., 2025b). The combination of FRP and SWSSC is of great significance for engineering construction and has attracted increasing attention.

The bending effect of concrete structures under load is one of the most significant effects (Sun et al., 2025). Thus, numerous scholars had studied the flexural performance of FRP-reinforced concrete beams to explore the failure characteristics of FRP- concrete beams (Lu et al., 2023b; Younis et al., 2020). The properties and failure mode of FRP significantly differ from those of steel. FRP has a higher tensile strength than traditional steel reinforcement but a lower elastic modulus, and FRP does not exhibit plastic deformation, which means there are no obvious warning signs before its failure. Thus, FRP-reinforced concrete beams exhibit brittle failure characteristics under flexural action.

Concrete material is an artificially mixed material, and its performance inevitably has variability. In structural design, it is necessary to consider the impact of performance variability on structural safety, usually based on reliability indicators and the degree of material performance variability, to obtain the partial coefficients of the material performance. For example, in the specification (GB 50010-2010, 2010), the material safety factor for concrete strength is 1.40; The materials factor is suggested as 1.50 in European standards; The American standard ACI 318 does not use partial factors, but instead uses strength reduction factors.

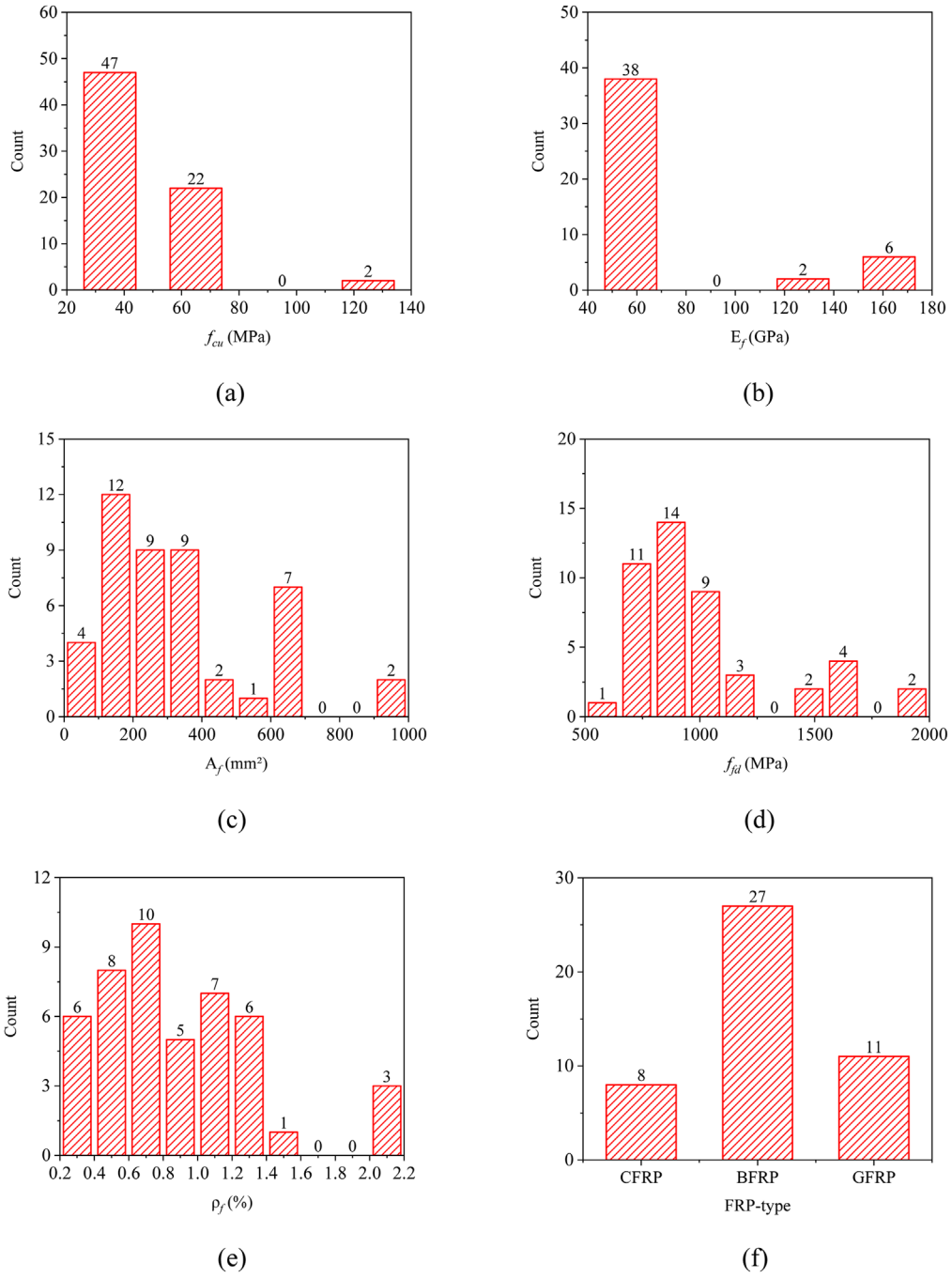

FIGURE 5
Distribution of database parameters. **(a)** Concrete compressive strength f_{cu} (MPa). **(b)** FRP elastic modulus E_f (GPa). **(c)** FRP tensile zone area A_f (mm^2). **(d)** FRP tensile strength f_{fd} (MPa). **(e)** Longitudinal reinforcement ratio ρ_f (%). **(f)** FRP-type.

However, there are performance differences between SWSSC and RC, which pose new requirements for the reliability assessment of FRP-SWSSC beams, and it is necessary to conduct a more detailed reliability assessment of FRP-SWSSC beams to obtain the partial factor for SWSSC.

To this end, this paper first collected 49 groups of FRP-SWSSC test data and analyzed the model uncertainty based on the bearing capacity calculation model provided by guideline (GB 50608-2020, 2020); Secondly, statistical characteristics of SSSWC were collected, and the ultimate state function for the flexural bearing capacity of FRP-SWSSC beams was established, and the reliability index calculation method based on MCS L-moment was introduced. Thirdly, the analysis was conducted on the parameter sensitivity of the reliability of the flexural bearing capacity of FRP-

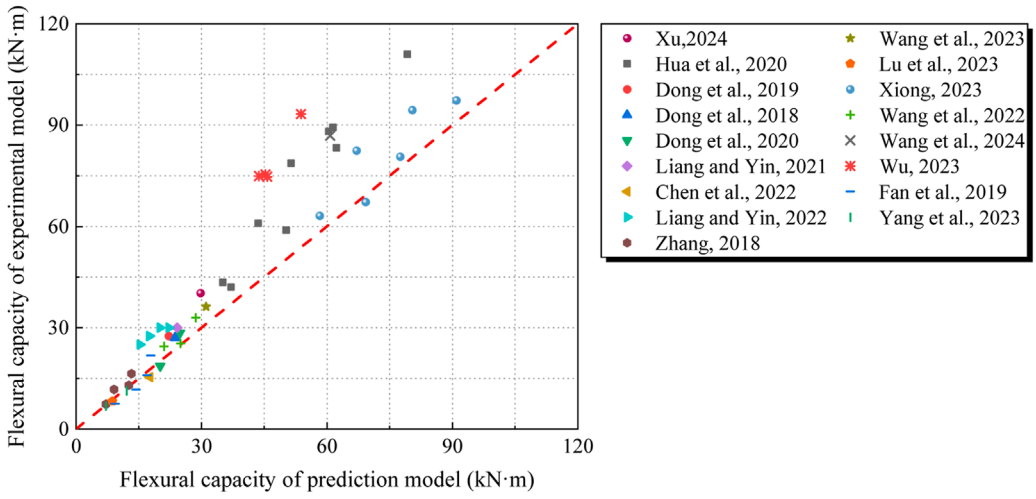

FIGURE 6
Comparison between the experimental and the predicted results.

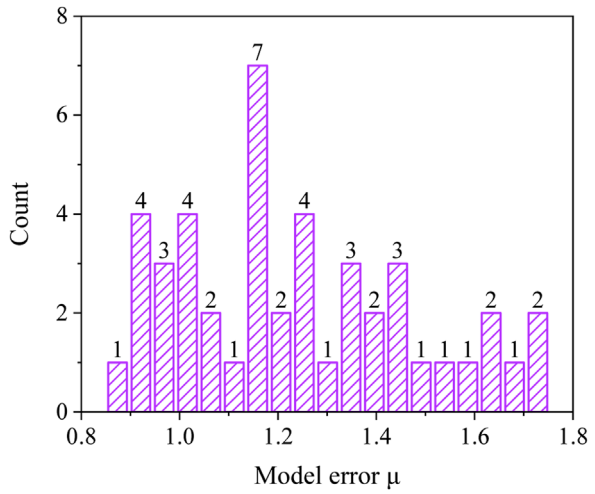

FIGURE 7
Distribution of model error.

TABLE 2 Results of Kolmogorov- Smirnov test.

Distribution	h value	p value
Normal	0	0.7182
Lognormal	0	0.9712
Extreme I	0	0.1739

SWSSC. Finally, the partial factor of SSSWC strength under a large number of conditions were calibrated, and reasonable partial factors were obtained.

TABLE 3 Load statistical parameters.

Load type	Bias	COV	Distribution	References
Dead load S_G	1.060	0.070	Normal	GB 50009-2012 (2012)
Live load $S_{Q,O}$	0.524	0.288	Type I	GB 50009-2012 (2012)
Live load $S_{Q,H}$	0.644	0.233	Type I	GB 50009-2012 (2012)

2 Flexural load capacity model of FRP-SWSSC

2.1 Prediction model

The flexural capacity prediction model recommended in the guideline (GB 50608-2020, 2020) was employed as the prediction model for the reliability analysis of FRP-SWSSC beams, and the model includes three types of failure modes for FRP-RC beams, which are tension failure, compression failure, and boundary failure.

In the case of tensile failure, the concrete has not yet reached its ultimate compressive strain, while the FRP reinforcement has already attained its ultimate tensile strain. The corresponding stress-strain distribution is illustrated in Figure 2 During compressive failure, the concrete is crushed after reaching its ultimate compressive strain, even though the FRP reinforcement has not yet reached its ultimate tensile strain, and the stress-strain distribution is shown in Figure 3. In the boundary failure condition, both the concrete and the FRP reinforcement reach their ultimate compressive and tensile strains nearly simultaneously. The corresponding stress-strain distribution is depicted in Figure 4.

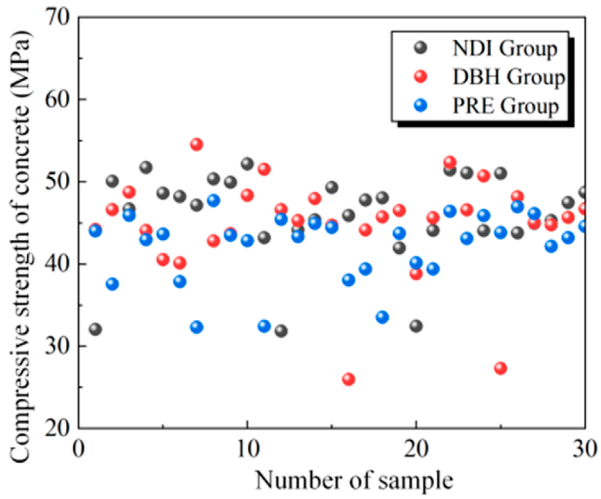

FIGURE 8
Strength of SSSWC samples from different region.

TABLE 4 Statistical parameters of SWSSC.

Material parameters	Bias	COV	Distribution
f_{cu}	1.2531	0.1228	Normal

According to the guideline (GB 50608-2020, 2020), the selection of different failure modes is based on the boundary reinforcement ratio ρ_{fb}, which is determined by Equation 1,

$$\rho_{fb} = \frac{\alpha_1 f_c}{f_{fd}} \cdot \frac{\beta_1 \varepsilon_{cu}}{\varepsilon_{cu} + \frac{f_{fd}}{E_f}} \tag{1}$$

where α_1 and β_1 represent the coefficients for the equivalent rectangular stress distribution in the concrete compression zone, which are determined according to the (GB 50010-2010, 2010). Here, ε_{cu} is the ultimate compressive strain of the concrete, with a value of 0.0033. According to the guideline (GB 50068-2018, 2018), the design value for the axial compressive strength of concrete, denote as f_c, is calculated using Equation 2.

$$f_c = \frac{f_{c,k}}{\gamma_f} \tag{2}$$

where γ_f is the partial factor for SWSSC, which will be calibrated through reliability analysis described later. $f_{c,k}$ is the specified value for the axial compressive strength of concrete. The standard value for the cubic compressive strength of concrete $f_{cu,k}$ can be converted to $f_{c,k}$.

The design value for the tensile strength of the FRP reinforcement, f_{fd}, is determined by using Equation 3 as specified in the guideline (GB 50608-2020, 2020).

$$f_{fd} = \frac{f_{(fd,k)}}{\gamma_{fe}\gamma_e} \tag{3}$$

where $f_{fd,k}$ is the standard value of the tensile strength of FRP bars, γ_{fd} is the partial factor for FRP bars, with a value of 1.25. γ_e is the environmental influence factor for FRP bars. The factors γ_e for different FRP bars under indoor conditions are obtained from Table 1.

For tensile failure, the guideline (GB 50608-2020, 2020) proposes that when the reinforcement ratio $\rho_f < 1.5\rho_{fb}$, the flexural member undergoes tensile failure, and the flexural capacity of the is calculated by using Equation 4,

$$M_u = A_f f_{fd}\left(h_0 - \frac{x}{2}\right) \tag{4}$$

where A_f is the cross-sectional area of longitudinal FRP reinforcement in the tensile zone; h_0 is the distance from the FRP reinforcement resultant point to the edge of the concrete compression zone; x is the height of the equivalent rectangular stress block in the concrete compression zone, determined by Equation 5,

$$x = \left[\frac{0.14}{1 + 400\left(\frac{f_{fd}}{E_f}\right)} + \frac{\rho_f f_{fd}}{f_c}\right] h_0 \tag{5}$$

where E_f is the elastic modulus of FRP reinforcement.

For compression failure, the guideline (GB 50608-2020, 2020) states that when the reinforcement ratio $\rho_f > 1.5\rho_{fb}$, the flexural member undergoes compression failure, and the flexural capacity can be calculated by the following formulas (Equations 6, 7),

$$M_u = A_f\left(\frac{\rho_f}{\rho_{fb}}\right)^{-0.55} f_{fd}\left(h_0 - \frac{x}{2}\right) \tag{6}$$

with

$$x = \frac{\rho_f f_c}{\alpha_1 f_c} h_0 \tag{7}$$

2.2 Model error

The prediction model was obtained by the theory and the experimental experience, and it inevitably leads to errors in the model. To comprehensively evaluate the reliability of flexural capacity of FRP-SWSSC beams and obtain the appropriate partial factor of SWSSC, the experimental results of 49 FRP-reinforced concrete beams were collected, as shown in Supplementary Appendix 2. The investigated parameters include concrete compressive strength f_{cu}, area of FRP bars A_f, elastic modulus E_f, tensile strength f_{fd}, reinforcement ratio ρ_f, and type of FRP. The distribution of material properties in the database is illustrated in Figure 5. The prediction model introduced in the above section was used to calculate the results corresponding to these parameters, and the model error μ is defined as Equation 8,

$$\mu = \frac{M_{(u,exp)}}{M_{(u,pre)}} \tag{8}$$

where $M_{u,exp}$ represents the experimental result, while $M_{u,pre}$ is the predicted result.

The comparison between the experimental and predicted results is shown in Figure 6, the mean value of μ is 1.177, with a coefficient of variation (COV) of 0.210, and it means that the model's predictions are slightly higher than the experimental values. The distribution

TABLE 5 Statistical parameters of FRP bars.

Material parameters	Bias	COV	Distribution	References
f_{fd}	1.09	0.05	Normal	Plevris et al. (1995)
E_f	1.0	0.05	Normal	Ribeiro and Diniz (2013)

TABLE 6 Statistical parameters of geometric parameters.

Geometric features	Bias	COV	Distribution	References
b	1	0.02	Normal	Guo et al. (2020)
h_0	1	0.02	Normal	Guo et al. (2020)
A_f	1	0.03	Normal	Zhang et al. (2022a)

TABLE 7 Partial factors.

Load type	GB 50010-2010 (2010)	ACI 318-19 (2019)	European Committee for Standardization (2002)	CSA A23.3:19 (2010)
γ_G	1.3	1.2	1.35	1.25
γ_Q	1.5	1.6	1.5	1.5

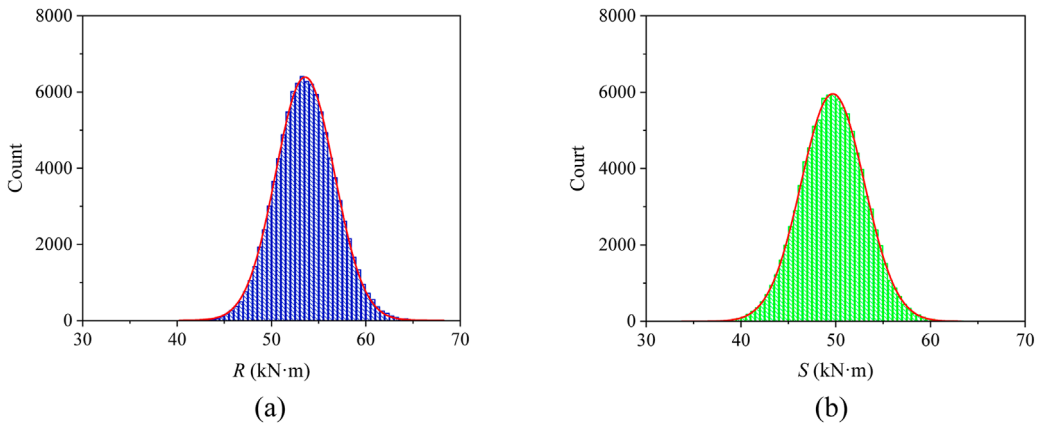

FIGURE 9
Resistance and load value distribution. **(a)** Resistance value distribution. **(b)** Load effect value distribution.

of the model error μ is illustrated in Figure 7. A hypothesis test using the Kolmogorov- Smirnov test was conducted to assess whether the data followed random distribution patterns, including normal, log-normal, and extreme value distributions. The results are presented in Table 2. The p-value is a probability measure used in hypothesis testing to determine whether to reject or fail to reject the null hypothesis. If the p-value is less than the chosen significance level (e.g., 0.05), the null hypothesis is rejected. An h-value of 1 indicates rejection of the null hypothesis (suggesting that the data do not follow the specified distribution), while an h-value of 0 indicates a failure to reject the null hypothesis. It can be seen that the sample does not reject the hypothesis, but from the distribution shape, its distribution state does not conform to the conventional distribution situation. Therefore, the L-moment statistical analysis method (Zhang W. et al., 2022) was used to characterize the distribution of model errors, and this method can be used to characterize random variables with atypical distribution patterns and generate more random samples. The first four linear moments of the model error were 1.1010, 0.1309, 0.0009956, and 0.0063, respectively, and more samples can be obtained by simulation according to these four values.

TABLE 8 Range of values for sensitivity analysis of beam parameters.

Key parameters	Retrieve value	Range values
b (mm)	175	100:50:250
h_0 (mm)	350	200:100:500
f_{cu} (MPa)	52.5	30:15:75
f_{fd} (MPa)	1,400	800:400:2000
E_f (GPa)	70	40:20: 100
A_f (mm^2)	175	100:50:250

3 Statistical parameters of random variables

In the design of concrete structures, two aspects of uncertainty need to be considered, namely, the uncertainty of effects and the uncertainty of resistance. Effects include internal forces (such as bending moments, shear forces, etc.) and deformation, mainly generated by load effects, and their uncertainty is also due to the uncertainty of loads. The uncertainty of resistance includes uncertainties in material properties, structural dimensions, and calculation models.

3.1 Load factors

According to the GB 50068-2018 (2018), two combinations can be used for analyzing structural reliability, which are $S_G + S_{Q,O}$ and $S_G + S_{Q,H}$. S_G represents the dead load and S_Q denotes the live load, the subscription "O" and "H" denotes office and house environments respectively. Table 3 lists the statistical parameters for the combination of dead load and live load.

3.2 Resistance factors

3.2.1 Material properties

Uncertainty in material properties mainly refers to the differences in material performance caused by factors such as process, loading, and environment. The reliability analysis in this paper involves material properties including the compressive strength of SWSSC, the elastic modulus of FRP bars, and the tensile strength of FRP bars.

In the work of Guo et al. (2020), 90 tests of SWSSC compressive performance were carried out, and the sea sands were from three regions in China (see Figure 8). The strength values ranged from 32.06 to 55.53 MPa. The statistical data were subjected to the K-S test protocol, indicating a good fit to a normal distribution, with none of the data rejecting the normal distribution hypothesis. The variability in the material properties of SWSSC can be represented by Equation 9,

$$\Omega_f = \frac{f_s}{f_{cu,k}} \tag{9}$$

where f_s represents the measured material property value of the specimen, while $f_{cu,k}$ denotes the standard material property value of the specimen, and it is obtained by using Equation 10,

$$f_{cu,k} = \mu_f - 1.645\sigma_f \tag{10}$$

where μ_f is the mean value of f_s, and σ_f is the standard deviation of f_s.

The mean value of Ω_f, which is the bias, and the COV of f_s can be obtained, as shown in Table 4.

The uncertainties of FRP bars were considered, including the uncertainties in the tensile strength and elastic modulus, and the statistical information of the two parameters can be found in Table 5.

3.2.2 Geometric parameters

The uncertainties in geometric parameters refer to the deviations in the geometric dimensions of the component cross-section caused by manufacturing and installation, among other reasons. The uncertainties of section width b, effective section height h_0, and FRP bar area A_f were considered, and the statistical information of these parameters can be found in Table 6.

4 Reliability analysis

In analyzing structural reliability, the primary load effects are the dead load effect S_G and live load effect S_Q, which are typically calculated first. These can be expressed as Equation 11,

$$S = S_G + S_Q \tag{11}$$

Due to the significant uncertainty associated with load effects, various design guidelines specify corresponding partial factors for dead load γ_G and live load γ_Q to ensure structural reliability, as shown in Table 7. The load effect can then be expressed as Equation 12,

$$S = \gamma_G S_G + \gamma_Q S_Q \tag{12}$$

Structural component parameters can be designed based on GB 50608-2020 (2020), where the resistance, or bending capacity M_u of SWSSC beams, can be calculated using Equations 4, 6. The limit state function of SWSSC beam can be written as Equation 13,

$$M_u(\gamma_0) \geq S_G(\gamma_G, \gamma_Q) \tag{13}$$

The calculation model of structural resistance can be regarded as relatively accurate. From an economic perspective, the ideal scenario is for the load effects to be perfectly aligned with the resistance, and thus the actual load effects can be expressed as Equation 14,

$$S = M_u \tag{14}$$

In the above equation, random variables are not taken into account. When considering the load partial factors, the actual resistance can be expressed as Equation 15,

$$M_u(\gamma_0, \gamma_G, \gamma_Q) = \gamma_G M_{u,G}(\gamma_0) + \gamma_Q M_{u,Q}(\gamma_0) \tag{15}$$

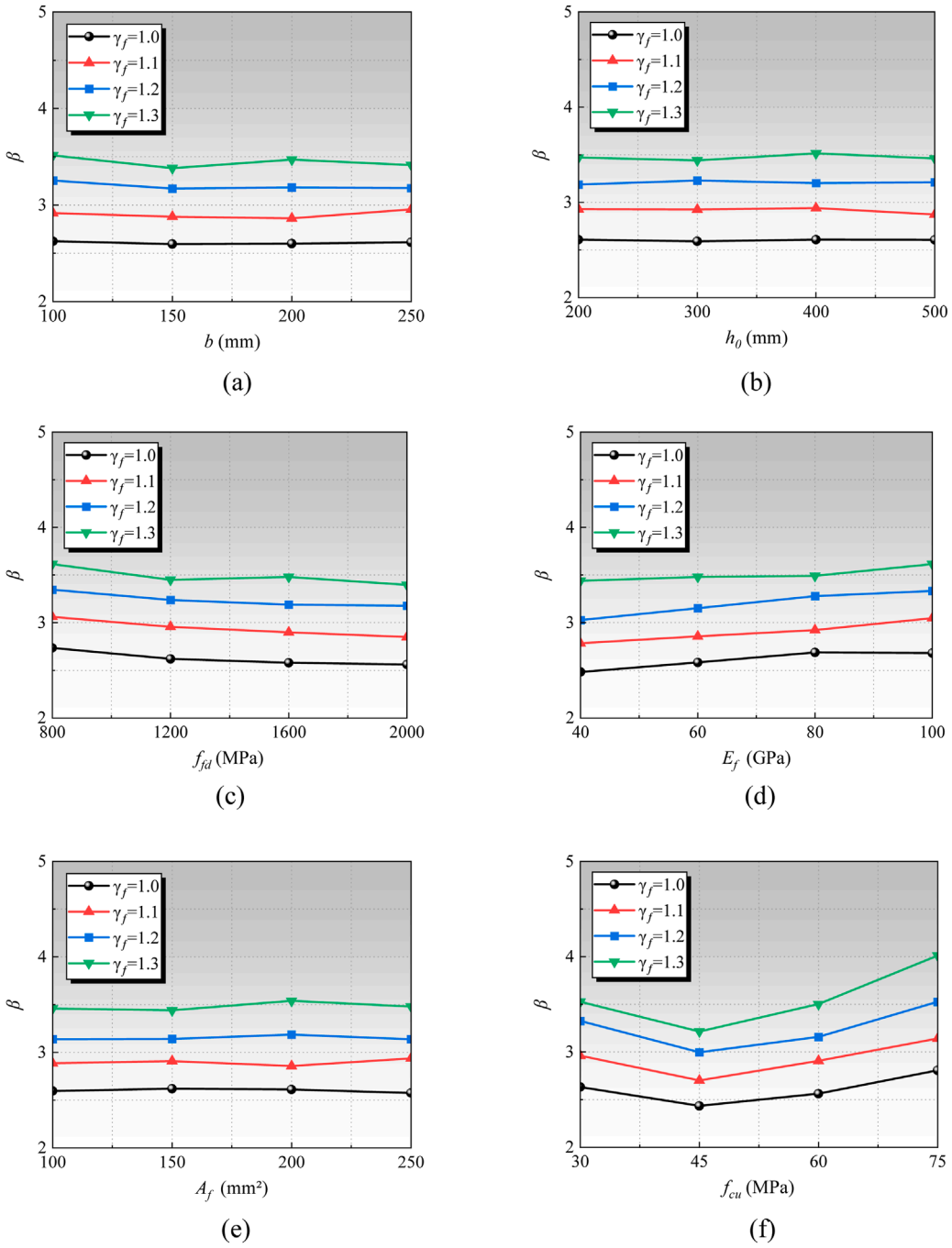

FIGURE 10
Reliability index with various parameter. **(a)** Section width b. **(b)** Effective height h_0. **(c)** FRP tensile strength f_{fd}. **(d)** FRP elastic modulus E_f. **(e)** FRP area A_f. **(f)** Concrete compressive strength f_{cu}.

where $M_{u,G}$ represents the portion of M_u that resists the dead load effects, while $M_{u,Q}$ denotes the portion that resists the live load effects. Assuming the ratio of dead load to live load was k, the Equations 16, 17 can be drawn,

$$M_{u,Q}(\gamma_0) = \frac{M_u(\gamma_0)}{1+k} \tag{16}$$

$$M_{u,G}(\gamma_0) = \frac{kM_u(\gamma_0)}{1+k} \tag{17}$$

Thus, Equation 18 can be rephrased as follows,

$$M_u(\gamma_0, \gamma_G, \gamma_Q) = \frac{\gamma_G M_u(\gamma_0)}{1+k} + \frac{\gamma_Q k M_u(\gamma_0)}{1+k} \tag{18}$$

TABLE 9 Parameters for sensitivity analysis of other factors.

Parameter	Retrieve value
b (mm)	100
h_0 (mm)	250
f_{cu} (MPa)	30
f_{fd} (MPa)	1800
E_f (GPa)	80
A_f (mm^2)	100

Furthermore, due to the discrepancies between the computational model and actual results, these errors need to be accounted for in the function, leading to the structural resistance equation being expressed as Equation 19,

$$M_u\left(\gamma_0,\gamma_G,\gamma_Q\right)=\frac{\mu\gamma_G M_u(\gamma_0)}{1+k}+\frac{\mu\gamma_Q kM_u(\gamma_0)}{1+k} \tag{19}$$

According to reliability theory, the limit state function can be rewritten as Equation 20,

$$Z=\frac{\mu\gamma_G M_u(\gamma_0)}{1+k}+\frac{\mu\gamma_Q kM_u(\gamma_0)}{1+k}-M_u \tag{20}$$

When $Z = 0$, the system is in equilibrium. A positive Z (i.e., $Z > 0$) indicates a safe state, whereas a negative Z (i.e., $Z < 0$) denotes an unsafe state. While the resistance carries inherent uncertainty, the load effects are treated as deterministic. Given that the resistance model is affected by multiple factors, the limit state function also displays uncertainty. The failure probability related to the limit state equation can be formulated as Equation 21,

$$P_f=P_r\left(Z<0\right) \tag{21}$$

The failure probability can be determined using the Monte Carlo simulation (MCS) method, and the failure probability p_f can be estimated using Equation 22,

$$p_f=\frac{n}{N} \tag{22}$$

where n denotes the number of failure samples, and N denotes the total number of samples, and in this study, 100,000 samples were used.

To quantify the failure probability p_f, the reliability index β was introduced, which had a direct mathematical relationship with the failure probability p_f, and it can be written as Equation 23,

$$\beta=\Phi^{-1}\left(1-p_f\right) \tag{23}$$

where Φ^{-1} is the inverse function of the cumulative distribution function of the standard normal distribution.

Additionally, based on the error distribution discussed in Section 2.2 and illustrated in Figure 7, it was observed that the model error μ does not follow a clear distribution pattern. Therefore, the L-moment statistical analysis method was employed for simulation. L-moments, a variant of traditional moments, serve as a statistical tool for measuring the characteristics of probability distributions (Zhang F. et al., 2022).

The simulation was conducted using a section width b of 150 mm, an effective height h_0 of 300 mm, concrete cubic compressive strength f_{cu} of 30 MPa, FRP tensile strength E_f of 1,200 MPa, FRP elastic modulus E_f of 80 GPa, FRP area A_f of 150 mm^2, partial factor γ_f of 1.0, and a k of 0.1. In this case, the partial factor was 1.0. A significant number of beam response samples were generated based on the known probability distributions of these random variables. Figure 9a presents the histogram of the resistance samples, and Figure 9b shows the histogram of the generated samples of the load effects, it can be seen that the distribution range of resistance is broader than that of the load effects, with most values exceeding the load effects. By subtracting the load effects S from the resistance R, the frequency of failure indexes that are less than or equal to zero was analyzed, leading to a calculated failure probability of 0.1948 for the structure.

5 Sensitivity analysis

Given that various variables in the computational space impact the reliability indexes of FRP-SWSSC beams to differing extents, a sensitivity analysis of these indexes is essential. This section will analyze the impact of the following factors on the reliability indexes section width b, effective section height h_0, concrete compressive strength f_{cu}, FRP bar tensile strength f_{fd}, FRP bar elastic modulus E_f, FRP bar reinforcement ratio A_f, national code load partial factors, FRP bar type, live load environment, SWSSC material partial factor γ_f, and the value k.

5.1 Sensitivity analysis of beam parameters

The parameters in the calculation model of flexural capacity of beam include b, h_0, f_{cu}, f_{fd}, E_f, and A_f. The sensitivity analysis parameter values are shown in Table 8. For the analysis, each parameter's range was set to 50% of its initial value, while others were derived from the parameter information space. For example, for parameter b, the initial value is 100 mm, with a variation of 50 mm, resulting in a range from 100 mm to 250 mm. The values for h_0, f_{cu}, f_{fd}, E_f, and A_f are respectively 350 mm, 52.5 MPa, 1400 MPa, 70 GPa, and 175 mm^2.

As shown in Figure 10, data analysis indicates that as γ_f increases, the reliability indexes also rise, and this is obvious because an increase in the material partial factor also means an increase in the material surplus, which further leads to an increase in the reliability index. Additionally, the effects of section width b, effective section height h_0, FRP bar tensile strength f_{fd}, FRP bar elastic modulus E_f, FRP bar reinforcement ratio A_f, on the reliability index β are relatively minor. The compressive strength of concrete f_{cu} has a significant impact on the reliability index, and the reliability index increases with the increase of concrete compressive strength. This is because the sensitivity of flexural bearing capacity to concrete compressive strength is relatively greater than other parameters.

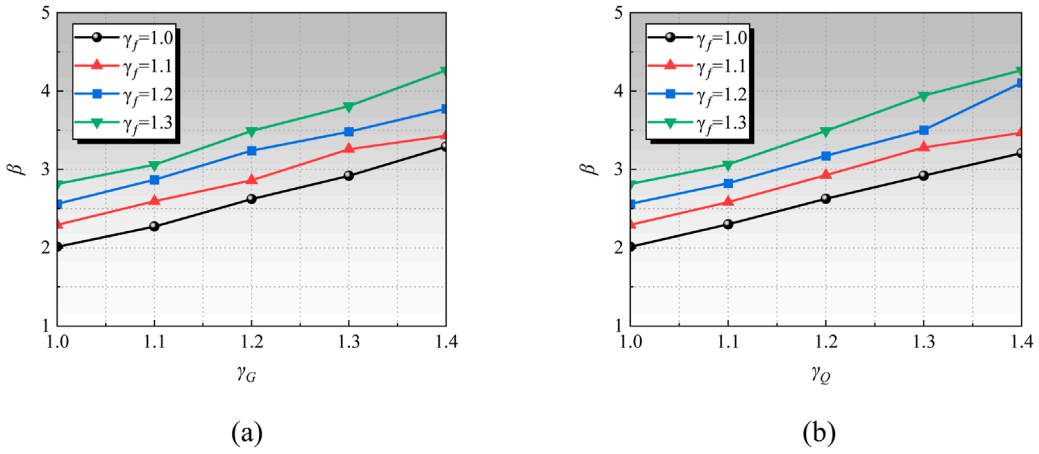

FIGURE 11
Influence of different load partial factors on reliability index. **(a)** Different live load partial factors. **(b)** Different dead load partial factors.

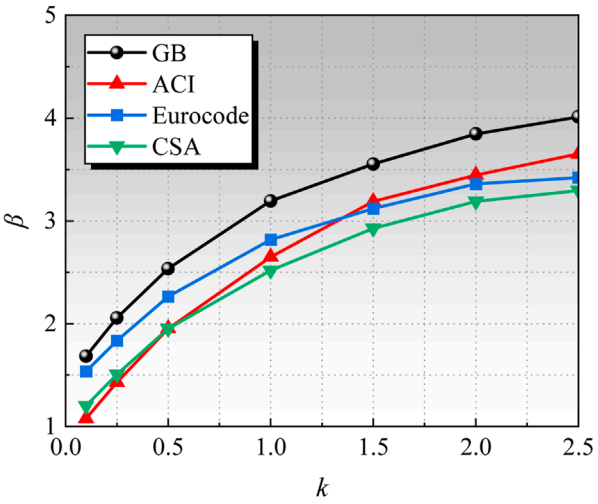

FIGURE 12
Influence of different k values on reliability index with different guideline.

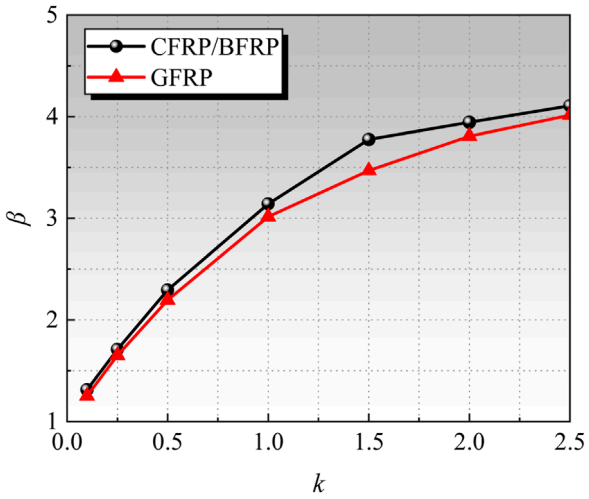

FIGURE 13
Influence of *k* value and FRP type on reliability index.

5.2 Other factors

5.2.1 Load partial factor

To compare the influence of different load partial factors on the reliability index, parameters were set as shown in Table 9, and *k* values 1. The load partial factors were taken at intervals of 0.1 from 1.0 to 1.4, and the results are shown in Figure 11 it can be observed that as the load partial factor increases, the reliability index also rises, and the rate of increase is similar, indicating that the load partial factor has a significant impact on the reliability index.

As illustrated in Figure 12, the Eurocode load partial factors benefit from a higher dead load partial factor, resulting in the highest overall reliability indexes. This indicates that, within the load partial factor values, this code provides the safest structural design, followed by the GB code and then the CSA code. Notably, as the live load proportion increases, the ACI code gradually surpasses the others in reliability indexes due to its higher live load partial factors, suggesting that under significant live-to-dead load effects, the structural design according to the ACI code is safer.

In addition, an increase in the ratio of dead load to live load significantly increases the reliability index. This is because the coefficient of variation of the dead load (0.070) is much smaller than that of the live load (0.288 or 0.233). As the proportion of the dead load increases, the dispersion of the load action becomes smaller, further leading to a larger reliability index.

5.2.2 FRP type

The relationship between the reliability indexes β of different types of FRP and the *k* value was analyzed, and the results can

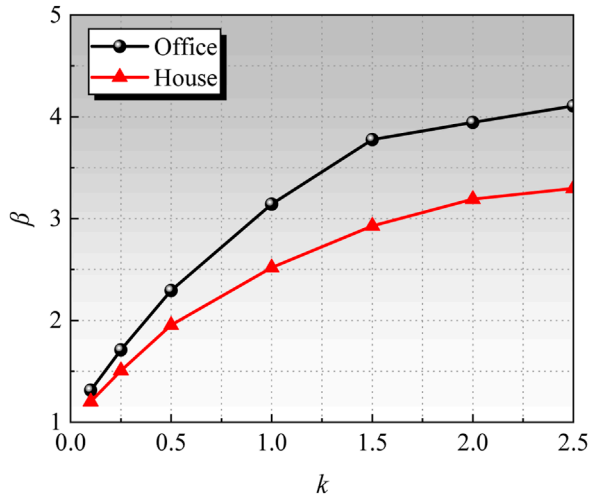

FIGURE 14
Influence of k value and environment type on reliability index.

TABLE 10 Calculation space.

Key parameters	Range values
b (mm)	100:50:250
h_0 (mm)	250:50:400
f_{cu} (MPa)	30:5:60
f_{fd} (MPa)	600:300:2400
E_f (GPa)	40:40:160
A_f (mm^2)	100:50:600

be found in Figure 13. Generally, the reliability indexes β for GFRP beam under various load effect ratios are lower than those for CFRP and BFRP beams. This phenomenon is attributed to differences in environmental impact coefficients between GFRP and CFRP/BFRP.

5.2.3 Live load environment

The relationship between the reliability index β under different environments and k value was analyzed, and the results are shown in Figure 14. It can be observed that the reliability index β increases with the increase of the material partial factor, and the rate of increase gradually diminishes. Comparing residential loads with office loads, it is found that the reliability index for office loads is slightly higher at the same value of k. This is mainly due to the larger deviation coefficient of residential loads compared to office loads, while the variation coefficients of both are fairly similar. Consequently, the uncertainty of residential loads is higher, leading to an increased probability of failure and a lower reliability index. In contrast, the office load has a smaller deviation coefficient, and the load values are relatively stable and predictable, resulting in a lower probability of failure and a higher reliability index.

6 Discussion of partial factor

6.1 Calculation space

Comprehensive structural reliability analysis requires designing a multi-dimensional calculation space. Therefore, this study considers the following parameters, concrete cube compressive strength f_{cu}, FRP bar tensile strength f_{fd}, FRP bar area A_f, FRP bar elastic modulus E_f, section width b, effective section height h_0, live load to dead load effect ratio k, and SWSSC material partial factor γ_f. Detailed information on the variation parameters for the FRP-SWSSC beam is provided in Table 10. There are six parameters in total, resulting in 29,568 design conditions based on the assigned values for each parameter. Additionally, the ratio k of live load to dead load significantly impacts the reliability of the beam, with k values set at 0.1, 0.25, 0.5, 1.0, 1.5, 2.0, and 2.5. To determine the SWSSC material partial factor γ_f, γ_f is varied from 1.0 to 1.8 with a step size of 0.05, resulting in 17 values. Consequently, 29,568 × 7 × 17 = 3,518,592 reliability calculations must be considered.

6.2 Calibration

In the process of calibrating the material partial factor γ_f for SWSSC, the target reliability index β_T must first be defined. The target reliability index is used to reflect the acceptable probability of structural failure for people. Taking a large number of ordinary buildings as an example, the standard (GB 50068-2018, 2018) stipulates that the target reliability index for ductile failure components is 3.2 (failure probability of 6.9×10^{-4}), and the target reliability index for brittle failure components is 3.7 (failure probability of 1.1×10^{-4}). Based on previous study (Zhang W. et al., 2022), the failure mode of FRP concrete beams under bending is brittle failure. Therefore, the target reliability index of 3.7 was determined.

In such cases, the material partial factor can be calibrated using the reliability calculation results from the design space to obtain the optimal γ_f value. To assess the closeness of the partial factor γ_f to the target reliability index β_T, the least squares method is employed. The formula is as follows,

$$H = \frac{1}{n}\sum_{i=1}^{n}(\beta_i - \beta_T)^2 \tag{24}$$

where H is the deviation value, n represents the number of design instances; β_i is the reliability index for the ith instance; β_T is the target reliability index. By using this method, the partial factor of SWSSC can be calibrated, that is, the smaller the H value, the more reasonable the partial factor.

Figures 15, 16 shown the deviation value of SWSSC partial factor with different type of FRP. It can be noted that when k = 0.5, 1.0, 1.5, 2.0 and 2.5 respectively, the value of H increases with k, while the deviation H does not show a significant characteristic with the increase of the partial factor γ_f, resulting in a relatively flat curve. When k = 0.1 and 0.25, the deviation H initially decreases

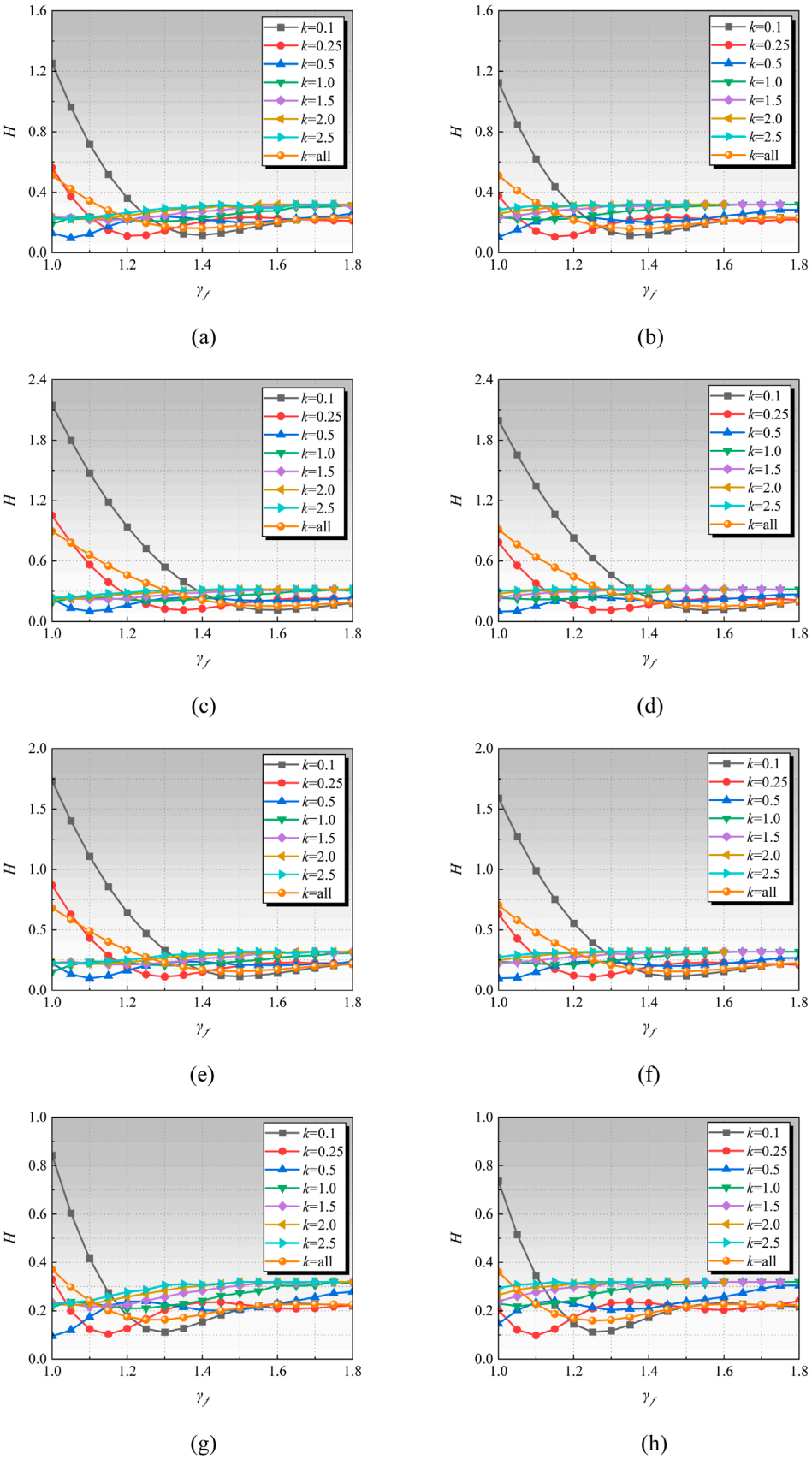

FIGURE 15
Deviation of CFRP/BFRP SWSSC partial factors. **(a)** GB-House. **(b)** GB-Office. **(c)** ACI-House. **(d)** ACI-Office. **(e)** CSA-House. **(f)** CSA-Office. **(g)** Eurocode -House. **(h)** Eurocode -Office.

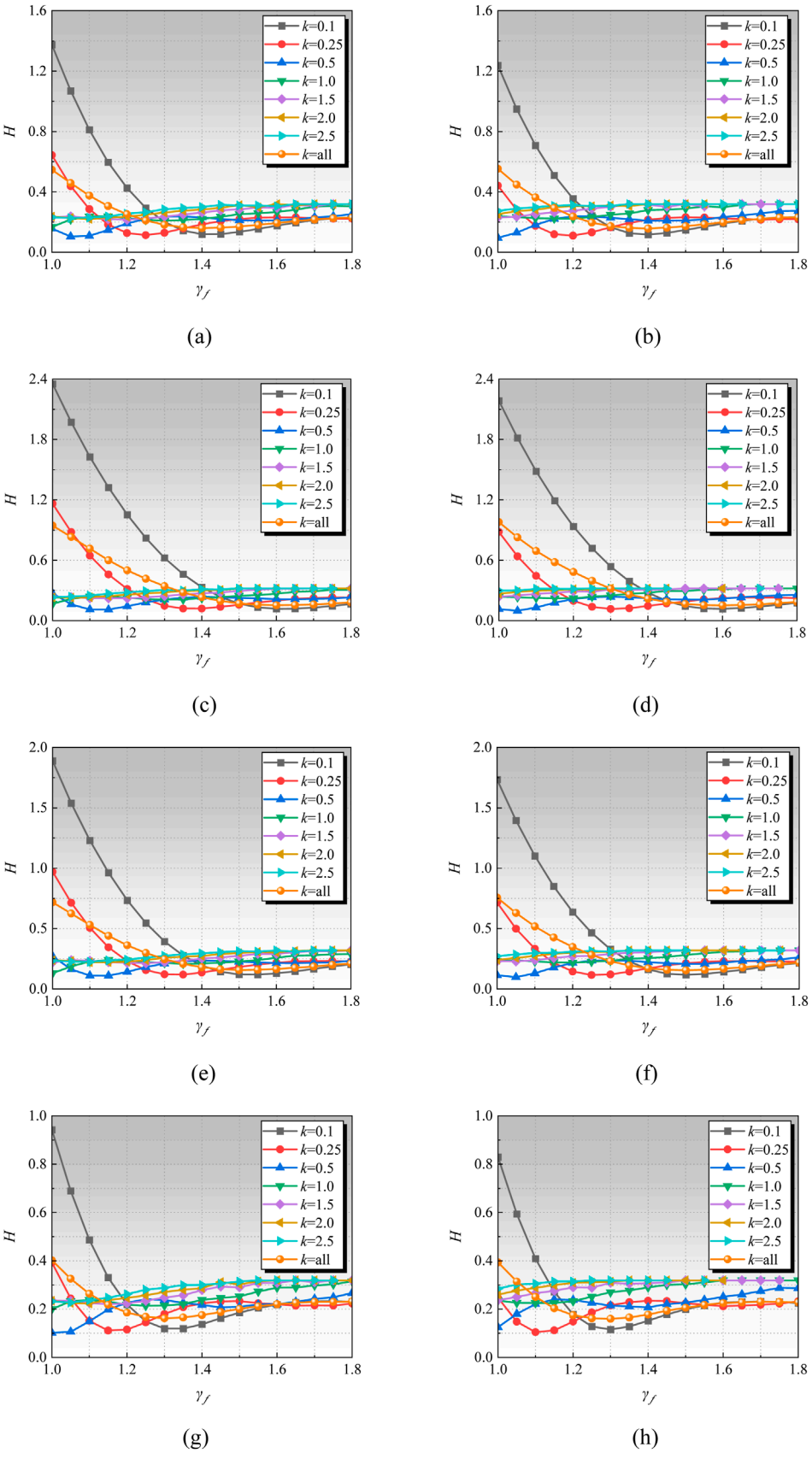

FIGURE 16
Deviation of GFRP SWSSC partial factors. **(a)** GB-House. **(b)** GB-Office. **(c)** ACI-House. **(d)** ACI-Office. **(e)** CSA-House. **(f)** CSA-Office. **(g)** Eurocode -House. **(h)** Eurocode -Office.

TABLE 11 Partial factors of SWSSC.

Load specification	FRP type	Live load environment	γ_f
GB	CFRP/BFRP	House	1.4
		Office	1.35
ACI		House	1.6
		Office	1.55
CSA		House	1.5
		Office	1.45
Eurocode		House	1.25
		Office	1.25
GB	GFRP	House	1.4
		Office	1.4
ACI		House	1.6
		Office	1.6
CSA		House	1.5
		Office	1.5
Eurocode		House	1.3
		Office	1.3

TABLE 12 Comprehensive recommendations for SWSSC partial factor.

Load specification	GB	ACI	CSA	Eurocode
γ_f	1.4	1.6	1.5	1.3

TABLE 13 Recommendations for SWSSC partial factor with various target reliability indexes.

Target reliability index	2.5	2.7	3.0	3.2	3.5	3.7	3.9
γ_f	1.15	1.20	1.25	1.30	1.35	1.4	1.45

and then increases with the increase of γ_f. For the condition k = 0.1, the minimum H value occurs when γ_f is 1.4, suggesting that the lowest deviation occurs when γ_f is set around 1.4. As γ_f increases beyond this point, the deviation also increases. Therefore, it is recommended that the load partial factor γ_f be set to 1.4. On this basis, for k = 0.25, the optimal value for γ_f is determined to be 1.2. The aforementioned method was applied to analyze other conditions, and the optimal material partial factors can be found in Table 11.

The recommended values for the SWSSC partial factor γ_f are listed under different load partial factor standards and varying live load environments. It can be observed that the recommended values are relatively close under different live load environments. In contrast, the influence of different load partial factor standards on the recommended values is significant. To facilitate the application of these analysis results in practical engineering, a comprehensive recommended value for the SWSSC partial factor γ_f under various load partial factor standards is provided in Table 12.

6.3 Partial factor with various target reliability index

The above analysis focuses on the situation where the target reliability index is 3.7. The target reliability index is artificially determined based on acceptable conditions and may vary in different periods and regions. Therefore, based on the above model, the material partial factor for different target reliability indexes (taking GB as an example) were calibrated. The target reliability indicators include 2.5, 2.7, 3.0, 3.2, 3.5, and 3.9. The recommended material partial factors for SWSSC after calibration are shown in Table 13.

7 Conclusion

To calculate the partial factors for SWSSC materials, this study examines the dependability of FRP-reinforced SWSSC beams utilizing experimental data from 49 groups worldwide. Using a thorough testing database, the uncertainty of the guideline (GB 50608-2020, 2020) model is evaluated. L-moments and Monte Carlo Simulation (MCS) are used in tandem to produce reliability indices. To assess how design variables affect average reliability indexes, a parameter analysis is carried out. Lastly, calibrated partial factors for SWSSC materials are suggested for two models using least squares averaging analysis in the design space. The following conclusions can be made in light of the results of this study and in-depth parameter studies:

1. According to the analysis, the prediction model's mean value is 1.117, and its coefficient of variation is 0.210. Furthermore, an examination of the SWSSC samples reveals that the normalized compressive strength SWSSC mean compressive strength is 1.2531 with a 0.1228 coefficient of variation.
2. Sensitivity analysis of the FRP-SWSSC beams indicates that factors such as the section width b, effective section height h_0, tensile strength of FRP bars f_{fd}, elastic modulus of FRP bars E_f, FRP reinforcement ratio A_f, and type of FRP have minimal impact on reliability.
3. During the sensitivity analysis, it was observed that when f_{cu} < 50 MPa, the reliability index decreases as f_{cu} increases. Conversely, when f_{cu} > 50 MPa, the reliability index increases with f_{cu}. A higher constant live load ratio k leads to greater reliability. Furthermore, under various load specifications, larger load partial factor corresponds to increased reliability. Additionally, under the same conditions in an office live load environment, reliability indexes are higher. Lastly, an increase

in the partial factor for SWSSC materials results in higher reliability indexes, demonstrating a linear relationship.

4. The following partial factors for SWSSC materials are suggested by an investigation of reliability indexes for FRP-SWSSC beams under different conditions: 1.4 for GB standards, 1.6 for ACI standards, 1.5 for CSA standards, and 1.3 for Eurocode standards.

This paper only discusses the reliability FRP SWSSC and and material partial factors of SWSSC under flexural effect, and the current model assumed a static condition. In addition, the structure is also subject to shear, torsion, serviceability (e.g., deflection, cracking), and long-term durability effect. The impact of these factors needs to be comprehensively considered in the design to determine reasonable material partial factors. Therefore, in future research, attention can be paid to this aspect to determine more comprehensive material partial factors. For static performance, the reliability model presented in this paper can be used for calculation. For long-term behavior, the degradation of concrete strength caused by factors such as carbonation can be considered. Due to the good durability of FRP reinforcement, its strength degradation does not need to be considered. However, if the structure is under fatigue load, the fatigue damage of FRP and concrete needs to be considered. It should be noted that the calibrated materials partial factor values were not validated against independent datasets or real-world case studies, and testing and verification can be conducted in practice in the future.

Data availability statement

The original contributions presented in the study are included in the article/Supplementary Material, further inquiries can be directed to the corresponding author.

Author contributions

SY: Writing – original draft. ZT: Conceptualization, Funding acquisition, Investigation, Writing – original draft. XL: Conceptualization, Investigation, Writing – original draft. HC: Data curation, Formal Analysis, Methodology, Validation, Writing – original draft.

Funding

The author(s) declare that financial support was received for the research and/or publication of this article. This work was supported by 2022 Open Fund Project of National Engineering Laboratory for Applied Technology of Forestry & Ecology in South China (2022NFLY01), Ningbo Polytechnic Faculty Recruitment Special Project (NZ24RC003) and the Natural Science Foundation of Fujian Province (2022J05184).

Conflict of interest

The authors declare that the research was conducted in the absence of any commercial or financial relationships that could be construed as a potential conflict of interest.

Generative AI statement

The author(s) declare that no Generative AI was used in the creation of this manuscript.

Any alternative text (alt text) provided alongside figures in this article has been generated by Frontiers with the support of artificial intelligence and reasonable efforts have been made to ensure accuracy, including review by the authors wherever possible. If you identify any issues, please contact us.

Publisher's note

Supplementary material

The Supplementary Material for this article can be found online at: https://www.frontiersin.org/articles/10.3389/fmats.2025.1677367/full#supplementary-material

References

ACI 318-19 (2019). *Building code requirements for structural concrete*. Farmington Hills, Michigan, USA: American Concrete Institute.

CSA A23.3:19 (2019). *Design of concrete structures*. Ottawa, Canada: CSA.

Dhondy, T., Remennikov, A., Asce, M., and Sheikh, M. N. (2024). Properties and application of sea sand in sea sand–seawater concrete. *J. Mater. Civ. Eng.* doi:10.1061/(ASCE)MT.1943-5533.00034

European Committee for Standardization (2002). *EN 1990:2002 – Eurocode – basis of structural design*. Brussels, Belgium: European Committee for Standardization (CEN).

Fahmy, M. F. M., Ahmed, S. A. S., and Wu, Z. (2021). Bar surface treatment effect on the bond-slip behavior and mechanism of basalt FRP bars embedded in concrete. *Constr. Build. Mater.* 289, 122844. doi:10.1016/j.conbuildmat.2021.122844

Fan, T.-H., Zeng, J.-J., Su, T.-H., Hu, X., Yan, X.-K., and Sun, H.-Q. (2025a). Innovative FRP reinforced UHPC floating wind turbine foundation: a comparative study. *Ocean. Eng.* 326, 120799. doi:10.1016/j.oceaneng.2025.120799

Fan, T.-H., Zeng, J.-J., Hu, X., Chen, J.-D., Wu, P.-P., Liu, H.-T., et al. (2025b). Flexural fatigue behavior of FRP-reinforced UHPC tubular beams. *Eng. Struct.* 330, 119848. doi:10.1016/j.engstruct.2025.119848

GB 50009-2012 (2012). *Load code for the design of building structures*. Beijing, China: Ministry of Housing and Urban-Rural Development of CHN.

GB 50010-2010 (2010). *Code for design of concrete structures*, Ministry of Housing and Urban-Rural Development of CHN, Beijing, China.

GB 50068-2018 (2018). *Unified standard for reliability design of building structures*. Beijing, China: Ministry of Housing and Urban-Rural Development of CHN.

GB 50608-2020 (2020). *Technical standard for fiber reinforced polymer (FRP) in construction*. Beijing, China: Ministry of Housing and Urban-Rural Development of CHN.

GB/T14684-2011 (2011). *Sand for construction*, Ministry of Housing and Urban-Rural Development of CHN.

Guo, M., Hu, B., Xing, F., Zhou, X., Sun, M., Sui, L., et al. (2020). Characterization of the mechanical properties of eco-friendly concrete made with untreated sea sand and seawater based on statistical analysis. *Constr. Build. Mater.* 234, 117339. doi:10.1016/j.conbuildmat.2019.117339

Han, S., Zhou, A., Fan, C., Xiao, G., and Ou, J. (2023). Axial-flexural performance of columns reinforced by steel-FRP composite bars and FRP ties. *Compos. Struct.* 322, 117435. doi:10.1016/j.compstruct.2023.117435

Hussein, A., Huang, H., Okuno, Y., and Wu, Z. (2022). Experimental and numerical parametric study on flexural behavior of concrete beams reinforced with hybrid combinations of steel and BFRP bars. *Compos. Struct.* 302, 116230. doi:10.1016/j.compstruct.2022.116230

Jafari, A., Shahmansouri, A. A., and Akbarzadeh Bengar, H. (2025). Hybrid CFRP-GFRP sheets for flexural strengthening of continuous RC beams: experimentation and analytical modeling. *Struct. Concr.* 26, 972–993. doi:10.1002/suco.202400264

Liao, J., Zeng, J.-J., Bai, Y.-L., and Zhang, L. (2022). Bond strength of GFRP bars to high strength and ultra-high strength fiber reinforced seawater sea-sand concrete (SSC). *Compos. Struct.* 281, 115013. doi:10.1016/j.compstruct.2021.115013

Lu, Z., Zhao, C., Zhao, J., Shi, C., and Xie, J. (2023a). Bond durability of FRP bars and seawater–sea sand–geopolymer concrete: Coupled effects of seawater immersion and sustained load. *Constr. Build. Mater.* 400, 132667. doi:10.1016/j.conbuildmat.2023.132667

Lu, Z., Li, W., Zeng, X., and Pan, Y. (2023b). Durability of BFRP bars and BFRP reinforced seawater sea-sand concrete beams immersed in water and simulated seawater. *Constr. Build. Mater.* 363, 129845. doi:10.1016/j.conbuildmat.2022.129845

Mai, G., Li, L., Lin, J., Wei, W., He, S., Zhong, R., et al. (2023). Bond durability between BFRP bars and recycled aggregate seawater sea-sand concrete in freezing-thawing environment. *J. Build. Eng.* 70, 106422. doi:10.1016/j.jobe.2023.106422

Miller, S. A., Horvath, A., and Monteiro, P. J. M. (2018). Impacts of booming concrete production on water resources worldwide. *Nat. Sustain* 1, 69–76. doi:10.1038/s41893-017-0009-5

Pan, D., Yaseen, S. A., Chen, K., Niu, D., Ying Leung, C. K., and Li, Z. (2021). Study of the influence of seawater and sea sand on the mechanical and microstructural properties of concrete. *J. Build. Eng.* 42, 103006. doi:10.1016/j.jobe.2021.103006

Panchanathan, A., and Paramasivam, A. (2022). Feasibility study on use of sea sand as partial replacemnt of fine aggregate in concrete. *Mater. Today Proc.* 65, 468–471. doi:10.1016/j.matpr.2022.03.016

Plevris, N., Triantafillou, T. C., and Veneziano, D. (1995). Reliability of RC members Strengthened with CFRP Laminates. *J. Struct. Eng.* 121, 1037–1044. doi:10.1061/(ASCE)0733-9445(1995)121:7(1037)

Ribeiro, S. E. C., and Diniz, S. M. C. (2013). Reliability-based design recommendations for FRP-reinforced concrete beams. *Eng. Struct.* 52, 273–283. doi:10.1016/j.engstruct.2013.02.026

Sun, H.-Q., Zeng, J.-J., Hong, G.-Y., Zhuge, Y., Liu, Y., and Zhang, Y. (2025). 3D-printed functionally graded concrete plates: Concept and bending behavior. *Eng. Struct.* 327, 119551. doi:10.1016/j.engstruct.2024.119551

Wang, X., Zhang, X., Ding, L., Tang, J., and Wu, Z. (2020). Punching shear behavior of two-way coral-reef-sand concrete slab reinforced with BFRP composites. *Constr. Build. Mater.* 231, 117113. doi:10.1016/j.conbuildmat.2019.117113

Wang, J., Xiao, F., and Yang, J. (2023). Experimental study on bond behavior between epoxy-coated reinforcement (ECR) and seawater sea-sand concrete (SSC) under FRP-steel confinement. *Constr. Build. Mater.* 385, 131426. doi:10.1016/j.conbuildmat.2023.131426

Wu, G., Lü, Z. T., and Wu, Z. S. (2006). Strength and ductility of concrete cylinders confined with FRP composites. *Constr. Build. Mater.* 20, 134–148. doi:10.1016/j.conbuildmat.2005.01.022

Younis, A., Ebead, U., Suraneni, P., and Nanni, A. (2020). Short-term flexural performance of seawater-mixed recycled-aggregate GFRP-reinforced concrete beams. *Compos. Struct.* 236, 111860. doi:10.1016/j.compstruct.2020.111860

Zeng, J.-J., Liao, J., Zhuge, Y., Guo, Y.-C., Zhou, J.-K., Huang, Z.-H., et al. (2022). Bond behavior between GFRP bars and seawater sea-sand fiber-reinforced ultra-high strength concrete. *Eng. Struct.* 254, 113787. doi:10.1016/j.engstruct.2021.113787

Zeng, J.-J., Sun, H.-Q., Deng, R.-B., Yan, Z.-T., and Zhuge, Y. (2025). Bond performance between FRP bars and 3D-printed high-performance concrete. *Structures* 73, 108377. doi:10.1016/j.istruc.2025.108377

Zhang, W., Liu, X., Huang, Y., and Tong, M.-N. (2022a). Reliability-based analysis of the flexural strength of concrete beams reinforced with hybrid BFRP and steel rebars. *Arch. Civ. Mech. Eng.* 22, 171. doi:10.1007/s43452-022-00493-7

Zhang, F., Feng, F., and Liu, X. (2022b). Reliability analysis of concrete beam with high-strength steel reinforcement. *Materials* 15, 8999. doi:10.3390/ma15248999

Zhang, Y., Hu, K., Zeng, J., and Hou, W. (2025). Long-term bond performance of fiber-reinforced polymer (FRP) bars to concrete in marine environments: a comprehensive review. *Arch. Civ. Mech. Eng.* 25, 118. doi:10.1007/s43452-025-01162-1